Regenerative Therapy 29 (2025) 455–465

Contents lists available at ScienceDirect

Regenerative Therapy

journal homepage: http://www.elsevier.com/locate/reth

Original Article

miR-145-enriched BMSCs-derived exosomes ameliorate neurogenic erectile dysfunction in aged rats via TGFBR2 inhibition

Yude Hong [a, b, 1], Zejia Feng [a, 1], Yunlong Ge [c, 1], Yuhang Xi [a], Bowen Zhang [a], Jianjie Wu [a], Tian Xia [a], Bowen Tang [d], Wei Wang [d], Jun Chen [d], Hua Wang [a, *], Hengjun Xiao [a, *]

[a] Department of Urology, The Third Affiliated Hospital of Sun Yat-Sen University, Guangzhou, China
[b] Department of Urology, The Second Affiliated Hospital, University of South China, Hengyang, China
[c] Department of Urology, The First Affiliated Hospital of Anhui Medical University, Hefei, China
[d] Department of Infertility and Sexual Medicine, The Third Affiliated Hospital of Sun Yat-sen University, Guangzhou, China

ARTICLE INFO

Article history:
Received 14 February 2025
Received in revised form
13 March 2025
Accepted 6 April 2025

Keywords:
Erectile dysfunction
Exosomes
miR-145
TGFBR2
Cavernous nerve injury

ABSTRACT

Background: Neurogenic erectile dysfunction (ED) is a prevalent complication following radical prostatectomy in elderly patients, primarily resulting from the apoptosis of corpus cavernosum smooth muscle cells (CCSMCs) and the subsequent excessive fibrosis of the corpus cavernosum.
Aim: This study aimed to compare the therapeutic effects of exosomes derived from lentivirus-transfected miR-145 bone marrow mesenchymal stem cells (Exo-145) and unmodified BMSCs-derived exosomes (Exo) in aged rats with bilateral cavernous nerve injury (BCNI) and investigate the underlying mechanisms.
Methods: Twenty-four-month-old male rats were assigned to four groups, namely Sham, BCNI, Exo, and Exo-145. Three weeks after treatment, erectile function was assessed by measuring the maximal intracavernosal pressure to mean arterial pressure (ICP/MAP) ratio. Apoptosis and fibrosis were semi-quantitatively analyzed using TUNEL and Masson's trichrome staining, respectively. In vitro, CCSMCs were subjected to H_2O_2-induced oxidative stress, and the protective effects of Exo-145 were evaluated through flow cytometry and Western blot. Lastly, the targets and mechanisms of miR-145 were further validated using dual-luciferase reporter assays and rescue experiments.
Results: Exo-145 significantly outperformed Exo in restoring erectile function in aged BCNI rats, as evidenced by the significantly higher maximal ICP/MAP ratio, a marked reduction in TUNEL-positive cell count, and marked suppression of fibrosis in cavernous tissue. Moreover, Masson's trichrome staining displayed a substantial decrease in collagen deposition. In vitro, Exo-145 alleviated H_2O_2-induced apoptosis in CCSMCs by downregulating Cleaved Caspase-3 expression and Bax while concurrently upregulating Bcl-2 expression. TGFBR2 was identified as a direct target of miR-145 through dual-luciferase reporter assays, with its overexpression partially reversing the protective effects of Exo-145.
Conclusion: Exo-145 demonstrates superior efficacy compared to Exo in treating aged neurogenic ED by targeting TGFBR2 to alleviate apoptosis and fibrosis. It may represent a promising cell-free therapeutic option for neurogenic erectile dysfunction in elderly patients and could offer new perspectives for improving their prognosis.

1. Introduction

Erectile dysfunction (ED), prevalent among men over 40 years, is defined as the persistent inability to achieve or maintain an erection sufficient for satisfactory sexual performance [1]. Neurogenic ED, resulting from the disruption of cavernous nerve signaling, constitutes a significant proportion of ED cases [2] and is

* Corresponding authors.
E-mail addresses: wangh585@mail.sysu.edu.cn (H. Wang), xiaohjun@mail.sysu.edu.cn (H. Xiao).
Peer review under responsibility of the Japanese Society for Regenerative Medicine.
[1] These authors contributed equally to this work.

https://doi.org/10.1016/j.reth.2025.04.004

particularly common among older patients following surgical interventions such as radical prostatectomy [3].

Despite significant research into ED treatment, oral phosphodiesterase type 5 inhibitors (PDE-5i) remain the primary treatment option [4]. However, their side effects and the inconsistent responses in a proportion of patients [5,6], highlight the need for more effective alternatives. Recently, mesenchymal stem cell-based therapies have garnered extensive attention within the field of regenerative medicine, including for the management of ED [7,8]. However, studies suggest their therapeutic effects are largely paracrine, not from direct cell replacement [9,10]. Exosomes, small extracellular vesicles mediating stem cell signaling via bioactive molecule transfer [11,12], offer a promising, innovative alternative to traditional cell-based therapies due to their capacity to promote tissue repair [13,14].

Prior studies have established that overexpressing miR-145 in bone mesenchymal stem cells (BMSCs) significantly alleviates age-related ED [15]. However, the underlying mechanisms of age-related ED and the precise role of miR-145 in neurogenic ED associated with aging remain elusive. Furthermore, clinical translation of miRNA therapies is hindered by RNase degradation and in vivo instability [16]. BMSC-derived exosomes offer a cell-free approach to address these limitations. Therefore, this study aims to investigate exosomes as miR-145 delivery vehicles, combining exosome therapy with miR-145 gene regulation.

In this study, an aged rat model of neurogenic ED induced by bilateral cavernous nerve injury (BCNI) was utilized to evaluate the therapeutic effects of exosomes derived from lentivirus-transfected miR-145 BMSCs (Exo-145) on erectile function. We hypothesize that Exo-145 alleviates ED by targeting key molecular regulators involved in fibrosis and apoptosis in cavernous tissue.

2. Materials and methods

2.1. Animals and grouping

Male Sprague-Dawley (SD) rats were acquired from the Laboratory Animal Center at Sun Yat-sen University and used in accordance with the guidelines of the Ethics Committee of Guangzhou Seyotin Biotechnology Co., Ltd. (Approval No. SYT2024082).

For this animal study, to ensure adequate statistical power, we determined the experimental sample size through a priori power analysis using the maximum intracavernous pressure/mean arterial pressure ratio (Max ICP/MAP) as the primary functional endpoint. The analysis was based on pooled data from our previous neurogenic erectile dysfunction (ED) studies conducted in our laboratory [15,17–19], which demonstrated mean Max ICP/MAP ratios ranging from 0.257 to 0.79 with standard deviations (SD) between 0.01 and 0.071. Based on the observed mean differences in Max ICP/MAP ratios from these comparable studies, we adopted a conservative approach by selecting the smallest detectable effect size for our calculations. Power analysis was performed using PASS software (version 15.0.5, NCSS LLC, USA) with a two-tailed significance level (α) of 0.05 and statistical power (1-β) set at 90 %. Power analysis indicated that a minimum sample size of four rats per group would be statistically sufficient to achieve the desired power. To enhance the robustness of our study and account for potential experimental variability or animal attrition, we conservatively chose to use six animals per group. This sample size is consistent with established sample sizes in similar preclinical investigations of neurogenic ED.

Subsequently, to evaluate the therapeutic efficacy of different treatments for neurogenic erectile dysfunction, twenty-four-month-old male rats with confirmed normal erectile function were randomized into four groups. The Sham group underwent sham surgery, involving exposure of the cavernous nerve without compression, and received intracavernosal injection of 200 μL phosphate-buffered saline (PBS). The BCNI group underwent bilateral cavernous nerve injury (BCNI) surgery to induce neurogenic erectile dysfunction, followed by intracavernosal injection of 200 μL PBS as a vehicle control. The Exo group received BCNI surgery and intracavernosal injections of 200 μg unmodified bone marrow-derived mesenchymal stem cell exosomes (Exo) dissolved in 200 μL PBS. Finally, the Exo-145 group received BCNI surgery and intracavernosal injections of 200 μg exosomes enriched with miR-145 (Exo-145), also dissolved in 200 μL PBS. Bilateral cavernous nerve injury (BCNI) surgery was performed as previously described [18]; briefly, the major pelvic ganglion (MPG) and cavernous nerve (CN) were identified based on anatomical landmarks, and the bilateral cavernous nerves were compressed using a vascular clamp for 2 min per side. In contrast, the Sham group underwent only nerve exposure without compression. Following surgery and foreskin retraction to expose the penis, intracavernosal injections were administered to all groups according to their assigned treatment regimen.

2.2. Erectile function assessment

Three weeks post-BCNI and the administration of either exosome or PBS, erectile function was evaluated as outlined in a previous study [18]. Under anesthesia, the right carotid artery and femoral trunk, along with the exposed bilateral CN, were exposed. Next, two 25-gauge catheters connected to pressure transducers (BL-420F, Techman Soft, China) were inserted into the carotid artery and the crus of the penis to simultaneously measure mean arterial pressure (MAP) and intracavernosal pressure (ICP). One catheter, inserted into the femoral trunk, was filled with a 250 U/mL heparin solution, while the other, inserted into the right carotid artery, contained a 25 U/mL heparin solution. Erectile function was assessed by calculating the ratio of maximal ICP to MAP.

2.3. Masson and immunohistochemical (IHC) staining

Mid-segment CC tissues were sequentially fixed in 4 % paraformaldehyde, dehydrated, and embedded in paraffin. Five-micron serial sections were then prepared for Masson's trichrome staining and IHC. Masson's trichrome staining was performed using a commercial kit (G1006, Servicebio). For IHC, tissue sections were dewaxed, rehydrated, and antigen-retrieved. They were then blocked with 5 % BSA (B265993, Aladdin) and incubated overnight at 4 °C with anti-α-SMA antibody (1:1000, 14395-1-AP, Proteintech). After incubation with secondary Ab, DAB staining was carried out, and the sections were visualized under a microscope.

2.4. TUNEL staining

Apoptotic cells in CC tissue were detected using the TUNEL assay (C1088, Beyotime) in accordance with the manufacturer's guidelines. Paraffin sections were dewaxed, exposed to proteinase K, and then cultivated in the presence of the TUNEL reaction mixture at 37 °C for 60 min. Sections were co-stained with DAPI and the examination was carried out using a fluorescence microscope.

2.5. Culture and transfection of miR-145-overexpressing BMSCs

Rat primary BMSCs (Cyagen Biosciences, Guangzhou, China) were cultured in Dulbecco's Modified Eagle's Medium (C11995500BT, Gibco) supplemented with 10 % fetal bovine serum (A3160801, Gibco) and 1 % penicillin/streptomycin (15140122, Gibco). Lentiviral vectors carrying miR-145 in combination with green fluorescent protein (GFP), along with a control GFP vector,

were synthesized by Hanbio Biotechnology (Shanghai, China). BMSCs were seeded into 6-well plates at a density of 5×10^5 cells per well and incubated overnight. The culture medium was then replaced with lentiviral particles (2.5×10^7 TU/mL, 1 mL) containing Polybrene (5 μg/mL). Following 4-h incubation at 37 °C, 1 mL of fresh complete medium was added. After 48 h, stably transfected cells were selected using complete medium containing puromycin (1 μg/mL) to establish miR-145-overexpressing BMSCs.

2.6. Exosome isolation and characterization

Exosomes were extracted from both BMSCs and miR-145-transfected BMSCs at approximately 70 % confluence. The cells were subsequently cultured for 48 h in a medium supplemented with 10 % exosome-depleted FBS. The exosome isolation protocol was performed as follows: Supernatants were sequentially centrifuged at 300×*g* and 2000×*g* for 10 min each to eliminate dead cells and debris. They were then further centrifuged at 10,000×*g* for 30 min. Exosomes were ultimately pelleted through two rounds of ultracentrifugation at 100,000×*g* for 70 min at 4 °C. The resulting pellet containing exosomes was resuspended and preserved at −80 °C.

To assess the morphology of the isolated exosomes, Transmission Electron Microscopy (TEM, FEI Tecnai G2 Spirit T12, Thermo Fisher Scientific, USA) was performed. For the identification of specific exosomal markers, Western blotting was carried out using antibodies against CD9 (1:1000; ab236630, Abcam), CD81 (1:1000; ab109201, Abcam), and TSG101 (1:1000; ab125011, Abcam). In addition, nanoparticle tracking analysis (NTA, ZetaView, Particle Metrix, Germany) was employed to determine the size distribution and concentration of the exosomes.

2.7. Isolation, culture, and lentiviral overexpression of TGFBR2 in CCSMCs

CCSMCs were isolated and cultured following a previously described method [19]. Briefly, the penises of 24-month-old rats were carefully collected. After removing tissues other than the CC, the remaining tissue was precisely sliced into 1–2 mm^3 segments. These segments were then evenly distributed on the bottom of a sterile 25 cm^2 culture flask (3289, Corning) and were maintained in high-glucose DMEM at 37 °C in a humidified atmosphere containing 5 % CO_2 until primary cells migrated from tissue explants and reached approximately 80 % confluence. CCSMCs were purified via differential adhesion. During passaging, non-adherent cells, which were CCSMCs, were removed by transferring the medium to new flasks within 30 min. This process was repeated twice to ensure purity. Third-generation CCSMCs were identified through immunofluorescence staining for desmin (1:200, 16520-1-AP, Proteintech) and α-smooth muscle actin (1:200, 14395-1-AP, Proteintech). For TGFBR2 overexpression, lentiviral vectors encoding TGFBR2 were transduced into CCSMCs following the protocol previously described for miR-145 mimic transfection.

2.8. Fluorescent labeling and exosomes internalization

Exosomes were stained with PKH67 (green) using the PKH67 Kit (UR52303, Umibio). Briefly, 80 μg of exosomes in 80 μL PBS were mixed with 1 μL PKH67 linker, diluted in 9 μL Diluent C, and thoroughly vortexed for 1 min. Thereafter, the mixture was incubated in the dark for 10 min. Subsequently, 35 mL PBS was added, following which the solution was centrifuged twice at 10,000×*g* for 70 min at 4 °C. The resulting pellet was resuspended with PBS. CCSMCs were then exposed to 20 μg/mL labeled exosomes for 24 h. DAPI staining was performed to visualize nuclei, and exosome internalization was observed through fluorescence microscopy (Nikon, Japan).

2.9. Apoptosis induction and cell viability assay

CCSMCs were plated in 96-well plates at a density of 5000 cells per well and cultured for 24 h. Oxidative stress was induced by exposing cells to 200–1000 μM H_2O_2 (CS7730, G-clone) for 4 h. Cell viability was assessed using a CCK-8 assay (CK04, DOJINDO), with absorbance measured at 450 nm (Spark 10 M, Tecan, Austria).

To investigate the protective properties of exosomes, CCSMCs were pretreated with various concentrations of exosomes for 24 h prior to H_2O_2 exposure. Apoptosis was evaluated via flow cytometry following Annexin V-FITC and PI double staining (BD FACSCanto™, USA), and FlowJo software was used for data analysis.

2.10. Quantitative real-time PCR (qRT-PCR)

Total RNA was isolated from samples using TRIzol Reagent (Invitrogen, 15596-026) and quantified with a Nanodrop One spectrophotometer (Thermo Fisher Scientific, USA). cDNA was synthesized using the cDNA Synthesis Kit (Vazyme, R323 for mRNA and MR101 for miRNA) according to the manufacturer's instructions. qRT-PCR was conducted with the SYBR Green PCR Kit (Vazyme, Q312 for mRNA and MQ102 for miRNA) on a LightCycler® 480 System (Roche, Switzerland). Gene expression levels were normalized to GAPDH for mRNA and U6 for miRNA. The sequences of primers used in this study are listed in Table 1.

2.11. Western blotting analysis

Proteins were extracted from CC tissues and CCSMCs using RIPA buffer supplemented with a protease inhibitor cocktail (KGB5101, KeyGEN). Protein concentrations were determined using a BCA kit (KGB2101, KeyGEN). The extracted proteins were separated by SDS-PAGE and transferred to PVDF membranes (IPVH00010, Millipore). Afterward, the membranes were blocked and then incubated overnight at 4 °C with primary antibodies against Cleaved Caspase 3 (1:10,000; 68773-1-Ig, Proteintech), Bax (1:10,000; 60267-1-Ig, Proteintech), Bcl-2 (1:1500; 26593-1-AP, Proteintech), TGFBR2 (1:10,000; 66636-1-Ig, Proteintech), and GAPDH (1:50,000; 60004-1-Ig, Proteintech). Protein bands were visualized using enhanced chemiluminescence (P10100, NCM Biotech) and captured using an imaging system (Tanon, China). For normalization, GAPDH served as the loading control. Band intensities of target proteins were quantified using ImageJ software and normalized to the band intensity of GAPDH in the same lane. The normalized protein expression levels were then used for statistical analysis.

Table 1
Primer sequences for RT-qPCR.

Gene	Sequence
miR145	Forward:5′-GCGGTCCAGTTTTCCCAGGA-3′ Reverse:5′-ATCCAGTGCAGGGTCCGAG-3′
TGFBR2	Forward:5′-CGACGTGACACTGTCCACTT-3′ Reverse:5′-AACTTGGGGTCGTGGCAAAC-3′
U6	Forward:5′-CTCGCTTCGGCAGCACA-3′ Reverse:5′-AACGCTTCACGAATTTGCGT-3′
GAPDH	Forward:5′-CAAGTTCAACGGCACAGTCAA-3′ Reverse:5′-TGGTGAAGACGCCAGTAGACTC-3′

2.12. Dual-luciferase reporter gene assay

The 3′UTR of TGFBR2 containing wild-type or mutated miR-145 binding sites was cloned into the psiCHECK-2 reporter vector (HanBio, Shanghai, China). Reporter constructs and miR-145 mimics or negative control were co-transfected into HEK-293T cells using Lipofectamine 3000 (L3000008, Invitrogen). After 48 h, luciferase activity was quantified using the Dual-Luciferase Reporter Gene Assay Kit (RG027, Beyotime).

2.13. Statistical analysis

Experiments were performed in triplicate for in vitro experiments. Statistical analysis was performed, and results are expressed as mean ± SEM. Statistical significance was determined using one-way ANOVA or Student's t-test. Statistical significance was set at $P < 0.05$.

3. Results

3.1. Characterization of BMSC-derived exosomes and miR-145 expression

Exosomes were successfully isolated and characterized. TEM revealed a round-shaped morphology (Fig. 1A), and NTA determined an average size of approximately 100 nm (Fig. 1B). Western blot analysis confirmed the presence of exosomal markers CD9, CD81, and TSG101 in exosomes, with lower expression observed in BMSCs and miR-145 mimic-transfected BMSCs (Fig. 1C). RT-qPCR demonstrated significantly higher miR-145 levels in BMSCs transfected with miR-145 mimic compared to the control and miR-145 NC groups (Fig. 1D). Correspondingly, exosomes from these BMSCs also displayed higher miR-145 levels (Fig. 1E), validating successful miR-145 enrichment in both BMSCs and their exosomes.

3.2. Characterization of CCSMCs and their interaction with BMSC-derived exosomes

Primary CCSMCs exhibited a spindle-shaped morphology after migrating from CC tissue explants (Fig. 2A). Differential adhesion effectively purified CCSMCs, as confirmed by immunofluorescence staining for α-SMA and Desmin (Fig. 2B). PKH67-labeled exosomes were successfully internalized by CCSMCs, as evidenced by green fluorescence within the cytoplasm (Fig. 2C). Additionally, co-culture with BMSC-derived exosomes resulted in a significant increase in miR-145 levels in CCSMCs (Fig. 2D).

3.3. Effect of exosomes on Erectile Function Recovery in BCNI SD rats

Erectile function, assessed by the ICP/MAP ratio, was significantly impaired in BCNI rats. However, treatment with Exo and Exo-145 markedly improved this ratio compared to the BCNI group, with Exo-145 exhibiting a more pronounced effect. (Fig. 3A and B).

3.4. Exosomes alleviate penile fibrosis and apoptosis in BCNI rats

Penile fibrosis was evaluated using Masson's trichrome staining and IHC for α-SMA. Masson's trichrome staining revealed that treatment with exosomes, particularly Exo-145, attenuated the loss of smooth muscle in cavernous tissue following CN injury, indicative of reduced fibrosis (Fig. 4A and B). Meanwhile, IHC analysis uncovered that the expression level of α-SMA was higher in the Exo-145 group compared to the Exo and BCNI groups, reflecting

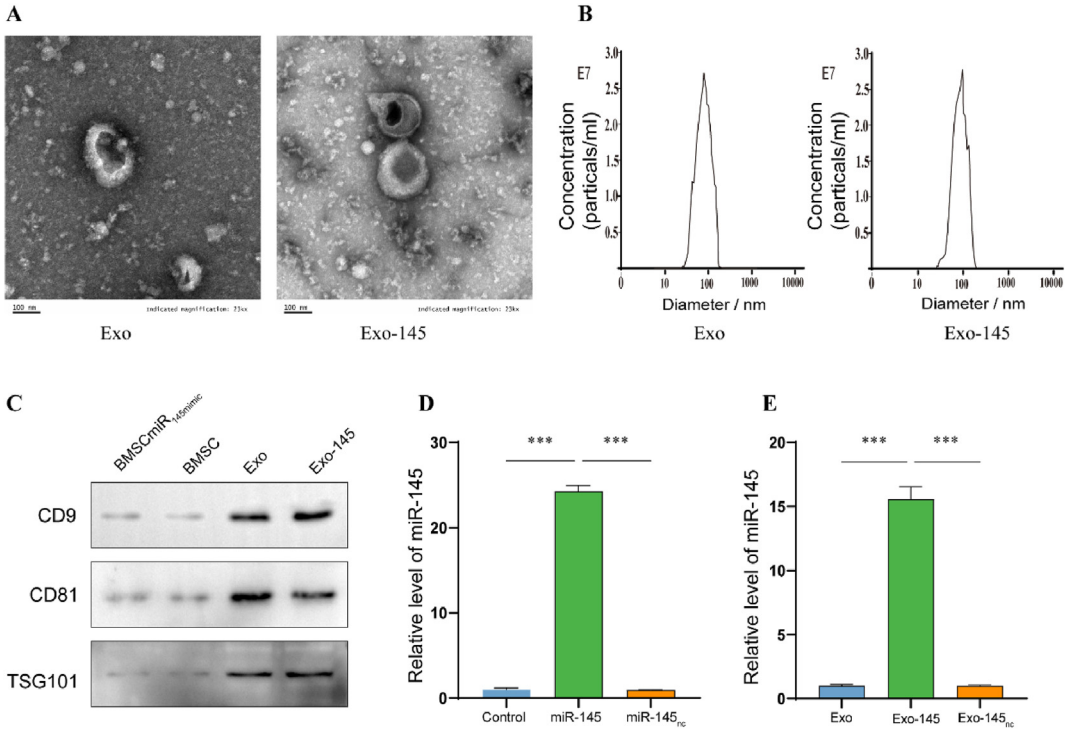

Fig. 1. Characterization of exosomes. (A) Transmission electron microscopy analysis of exosomes (scale bar = 100 nm). (B) Size distribution of exosomes as determined by nanoparticle tracking analysis. (C) Western blot analysis of exosomal markers CD9, CD81, and TSG101 in BMSCs and exosomes. (D) Elevated miR-145 levels in miR-145 mimic-transfected BMSCs compared to control and miR-nc groups (n = 3). (E) RT-qPCR of miR-145 levels in exosomes (n = 3), showing significant enrichment in miR-145 mimic-transfected BMSCs and Exo-145 group compared to controls. Data are presented as mean ± SEM. ***$p < 0.001$.

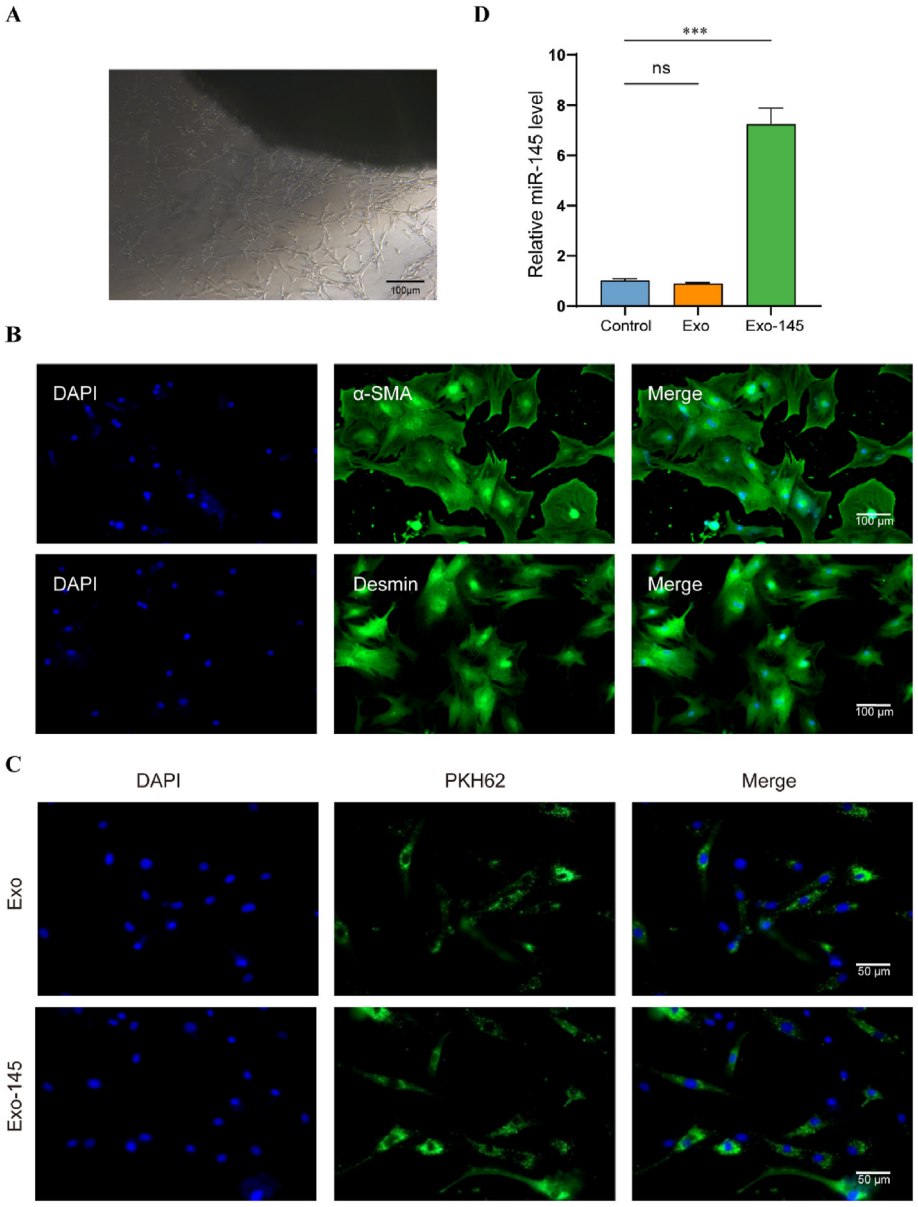

Fig. 2. Characterization of CCSMCs and their interaction with exosomes. (A) Primary CCSMCs migrating from cavernous tissue explants. (B) Immunofluorescence staining with anti-α-SMA and anti-Desmin antibodies confirming the identity of CCSMCs. (C) Internalization of PKH67-labeled Exo and Exo-145 by CCSMCs, showing green fluorescence within the cytoplasm. (D) Elevated miR-145 expression levels in CCSMCs after co-culture with Exo or Exo-145. Data are presented as mean ± SEM. ***$p < 0.001$, ns: no significant difference.

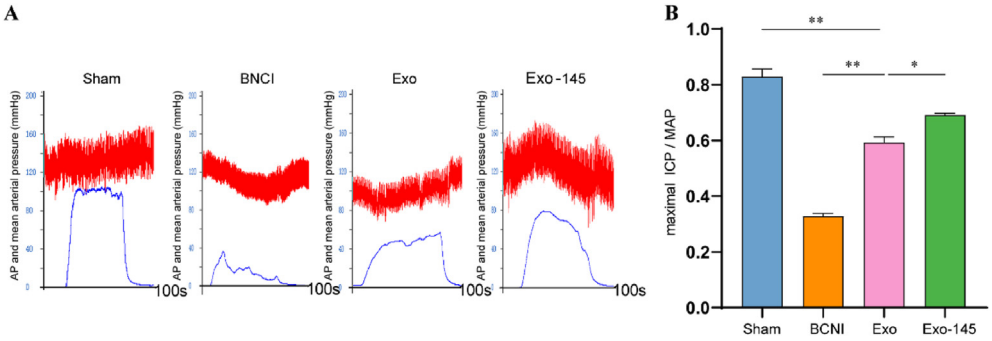

Fig. 3. Impact of Exosomes on Erectile Function Recovery in BCNI SD Rats. (A) Representative tracings of ICP and arterial pressure responses during cavernous nerve electrical stimulation three weeks post-surgery. (B) Maximal ICP/MAP ratio among the sham, BCNI, Exo, and Exo-145 groups (n = 6). Data are presented as mean ± SEM. *$p < 0.05$, **$p < 0.01$.

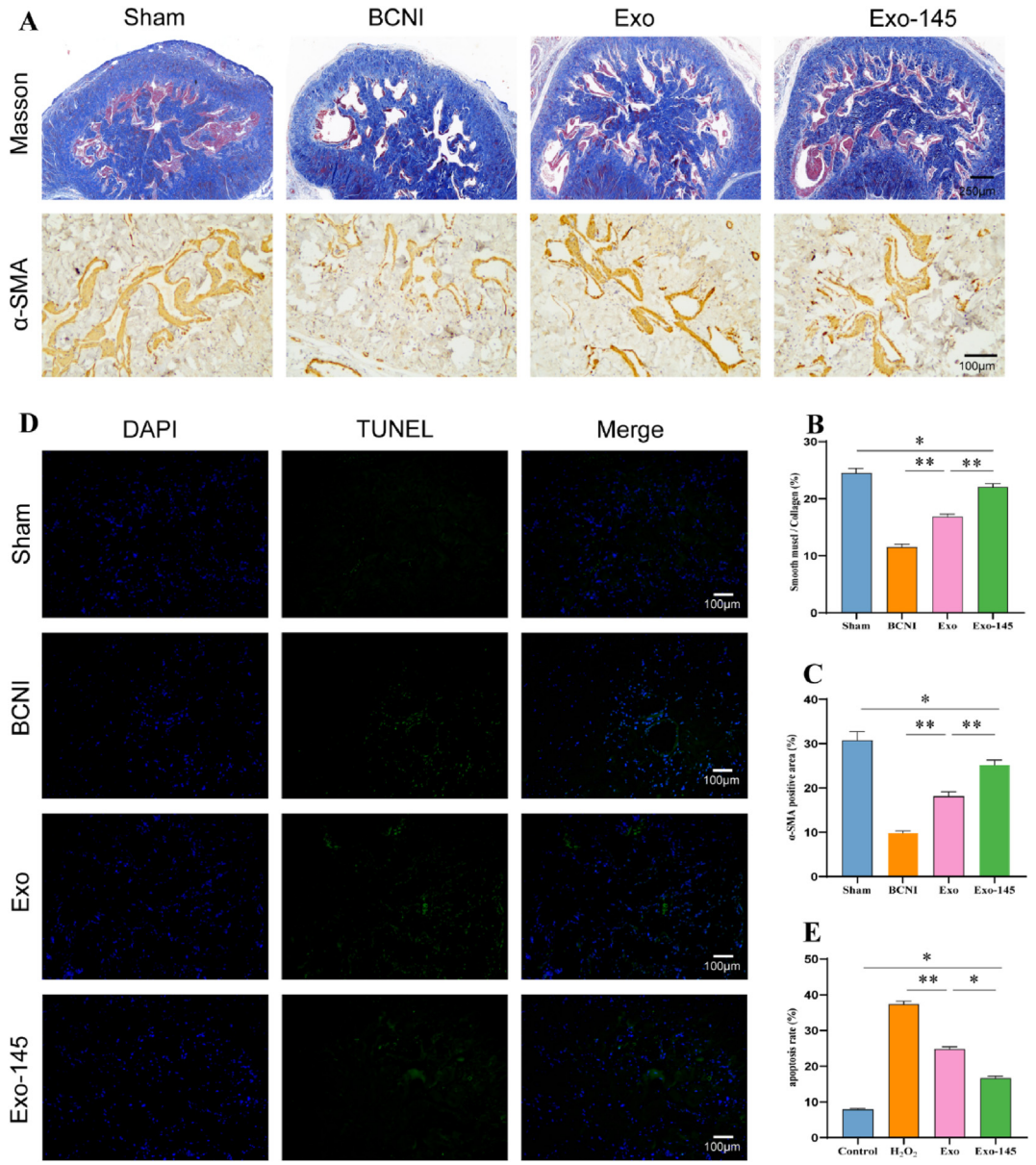

Fig. 4. Effects of exosome treatment on penile fibrosis and apoptosis in aged BCNI rats. (A) Masson's trichrome staining (red: smooth muscle; blue: collagen) and α-SMA immunohistochemical staining of cavernous tissue. (B) Smooth muscle-to-collagen ratio in cavernous tissue (n = 6). (C) Quantification of α-SMA-positive areas in cavernous tissue (n = 6). (D) TUNEL staining (green: TUNEL; blue: DAPI) showing apoptosis. (E) Percentage of TUNEL-positive cells (n = 6). Data are presented as mean ± SEM. *$p < 0.05$, **$p < 0.01$.

enhanced smooth muscle content and reduced fibrosis (Fig. 4A and C). Additionally, TUNEL staining demonstrated increased apoptosis in CC tissue following BCNI, while exosome treatment, especially Exo-145, significantly alleviated apoptosis (Fig. 4D and E).

3.5. Exosome-mediated protection against H_2O_2-induced CCSMC apoptosis in vitro

CCSMCs treated with H_2O_2 exhibited reduced viability. According to the results of the CCK-8 assay, cell viability significantly decreased at 800 μM H_2O_2 (Fig. 5A). Thus, this concentration was selected to evaluate the protective effects of exosomes. Co-incubation of CCSMCs with 20 μg/mL exosomes for 24 h significantly attenuated H_2O_2-induced inhibition of cell viability, with Exo-145 exerting a more pronounced protective effect compared to standard exosomes. Notably, concentrations higher than 20 μg/mL did not lead to further improvement in cell viability. Consequently, 20 μg/mL Exo or Exo-145 was selected for the ensuing experiments (Fig. 5B). Flow cytometry validated that Exo-145 significantly reduced H_2O_2-induced apoptosis in CCSMCs (Fig. 5C and D), and Western blot analysis further corroborated these findings, showing that Exo-145 treatment decreased the expression level of pro-apoptotic proteins Cleaved Caspase-3 and Bax while increasing that of the anti-apoptotic protein Bcl-2 (Fig. 5E–H).

3.6. miR-145-enriched exosomes attenuate CCSMC apoptosis via TGFBR2 regulation

To investigate the molecular mechanism underlying the protective effect of Exo-145, TargetScan [20], miRWalk [21], and miRDB [22] were used to predict the potential target genes of miR-

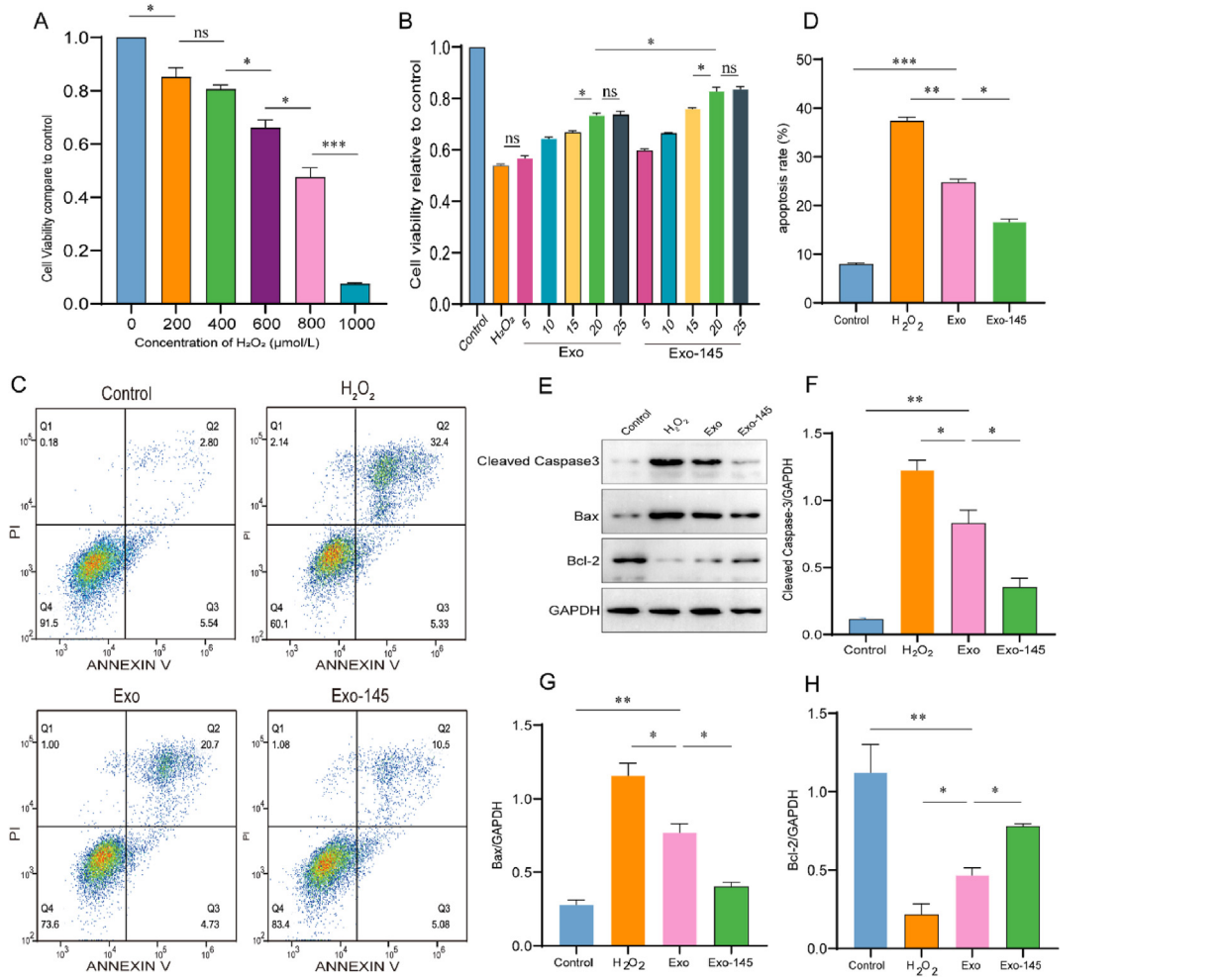

Fig. 5. Exosome-mediated protection against H2O2-induced CCSMC apoptosis in vitro. (A) CCK-8 assay showing CCSMC viability after treatment with various concentrations of H_2O_2 (0, 200, 400, 600, 800, and 1000 μM) for 4 h. (B) CCK-8 assay of CCSMC viability after pretreatment with 5, 10, 15, 20, or 25 μg/mL Exo or Exo-145 for 24 h, followed by 800 μM H_2O_2 treatment for 4 h. (C) Flow cytometry analysis of apoptosis in CCSMCs treated with PBS (Control), H_2O_2 alone, Exo + H_2O_2, or Exo-145 + H_2O_2. (D) Quantification of apoptotic cells from flow cytometry data. (E–H) Expression levels of Cleaved Caspase-3, Bax, and Bcl-2 analyzed by Western blot in CCSMCs. GAPDH was used as an internal/loading control. Data are presented as mean ± SEM. *$p < 0.05$, **$p < 0.01$, ***$p < 0.001$, ns: no significant difference.

145. Bioinformatic analysis yielded nine candidate targets, among which TGFBR2, PDCD4, and KLF4 were prioritized for experimental validation. qRT-PCR validation identified TGFBR2 as the most probable direct target, showing the most significant expression modulation (Fig. 6A and Fig. S1). Notably, pretreatment with Exo-145 substantially attenuated H_2O_2-induced TGFBR2 upregulation in CCSMCs (Fig. 6B), suggesting miR-145-mediated transcriptional regulation. This interaction was further confirmed by luciferase reporter assays, wherein mutation of the predicted miR-145 binding site completely abrogated the regulatory effect (Fig. 6C).

To establish the functional relevance of TGFBR2 in miR-145-mediated cytoprotection, TGFBR2-overexpressing CCSMCs were generated via lentiviral transduction. Successful overexpression was verified at the mRNA level (Fig. 6D). As anticipated, TGFBR2 overexpression markedly compromised Exo-145's anti-apoptotic efficacy, as evidenced by flow cytometric quantification of apoptotic cells (Fig. 6E and F) and immunoblotting analysis of apoptosis markers. Besides, the Exo-145-induced down-regulation of Cleaved Caspase-3 and Bax, along with Bcl-2 upregulation, was significantly reversed in TGFBR2-overexpressing cells following H_2O_2 challenge (Fig. 6G–J). Extending these findings to an in vivo context, age-associated elevation of TGFBR2 expression was observed in the BCNI group, which was effectively normalized by exosome treatment in aged ED rats (Fig. 6K-L).

Collectively, our multi-modal experimental approach demonstrated that TGFBR2 is the predominant downstream effector of miR-145, mechanistically linking exosomal miRNA delivery to both apoptosis inhibition and functional recovery in age-related ED complicated by BCNI.

4. Discussion

This study demonstrates the therapeutic efficacy of Exo-145 in aged rats with neurogenic ED following cavernous nerve injury (BCNI). Our prior work revealed a key age-related difference: while young rats spontaneously recover corpus cavernosum smooth muscle and erectile function post-BCNI within 8 weeks, aged rats develop persistent ED due to impaired regeneration and sustained cavernosal cell apoptosis [19]. The clinical significance of this age-related difference is underscored by the convergence of global population aging and rising prostate cancer incidence,

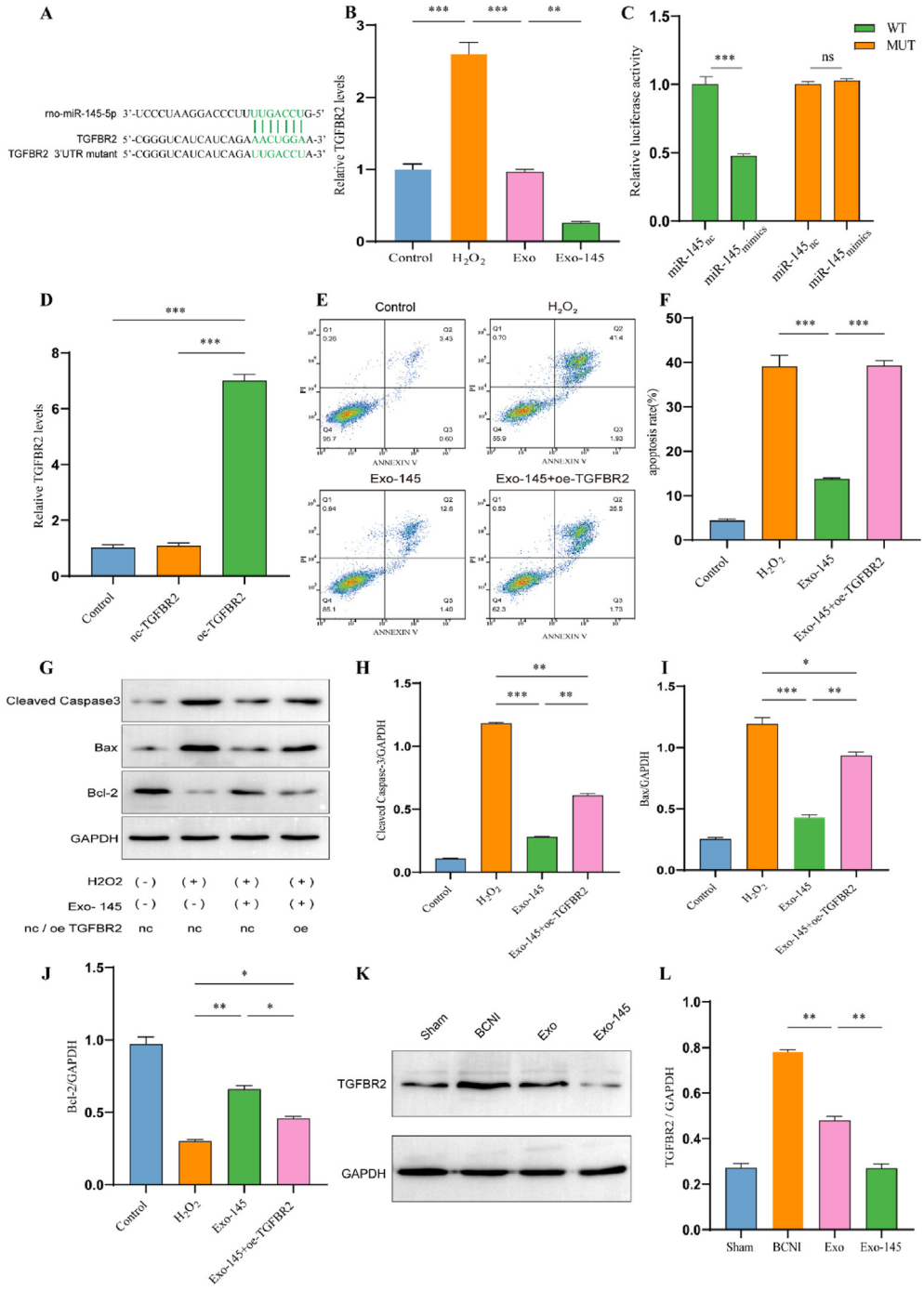

Fig. 6. Exo-145 modulates CCSMCs apoptosis via TGFBR2. (A) Schematic illustration of the predicted binding sites between miR-145 and the 3′ untranslated region (UTR) of TGFBR2. (B) qPCR analysis of TGFBR2 expression in CCSMCs after H_2O_2 stimulation following pretreatment with PBS, Exo, or Exo-145. (C) Luciferase activity assay in CCSMCs transfected with wild-type or mutant TGFBR2 3′ UTR and miR-145 mimics or negative control (nc). (D) qPCR results following transfection of TGFBR2 mimics in CCSMCs. (E-F) Flow cytometry analysis of apoptosis in TGFBR2-overexpressing CCSMCs treated with Exo-145 and H_2O_2. (G-J) Western blot analysis of Bax, Bcl-2, and Cleaved Caspase-3 protein levels in H_2O_2-induced CCSMCs co-incubated with exosomes, showing the impact of TGFBR2 overexpression on apoptotic regulation. (K-L) Western blot analysis of TGFBR2 protein levels in cavernous tissue (n = 3). In Western blot experiments, GAPDH was used as an internal/loading control. Data are presented as mean ± SEM. *$p < 0.05$, **$p < 0.01$, ***$p < 0.001$, ns: no significant difference.

synergistically driving an epidemic of postoperative neurogenic ED [23,24]. Despite these challenges, therapeutic development remains disproportionately focused on younger preclinical models.

To address this translational gap, a rigorously validated 24-month-old rat model corresponding to the physiological state of 60-year-old humans and recapitulating the molecular constraints of geriatric tissue repair was constructed [25]. In this pathophysiologically relevant system, Exo-145 administration restored erectile function, as evidenced by normalized maximal ICP/MAP ratios, while concurrently reversing hallmark pathological features of ED progression, namely cavernosal apoptosis and collagen deposition. Noteworthily, these therapeutic outcomes not only validate our mechanistic targeting strategy but also demonstrate age-specific efficacy, a vital aspect of clinical translation.

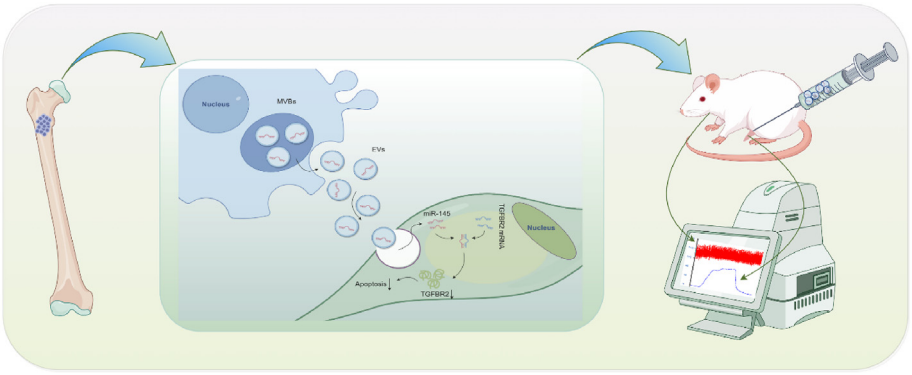

Fig. 7. Mechanism by which Exo-145 alleviates erectile dysfunction following BCNI. Exo-145 delivers miR-145 to CCSMCs, targeting TGFBR2 to reduce apoptosis and fibrosis, thereby improving erectile function.

A crucial aspect of Exo-145's therapeutic efficacy is its function as an efficient miRNA delivery system. Indeed, while miRNAs possess potent regulatory capabilities, their effective in vivo administration necessitates a stable and biocompatible carrier. Exosomes serve as natural carriers that protect miRNAs from RNase-mediated degradation, thereby enhancing their therapeutic potential [26]. Owing to their high biocompatibility, efficient cellular uptake, and intrinsic ability to transfer functional miRNAs, these vesicles have emerged as an optimal platform for miRNA-based therapies [27,28]. Our study confirms that miR-145 was successfully enriched in BMSC-derived exosomes following lentiviral transfection, and these engineered exosomes (Exo-145) efficiently transferred miR-145 into CCSMCs, as evidenced by RT-qPCR analysis and fluorescently labeled exosome tracking experiments. The direct uptake of Exo-145 by CCSMCs, along with the subsequent increase in intracellular miR-145 levels.

miR-145 is a master regulator of smooth muscle cell fate, modulating apoptosis and fibrosis in various tissues [29]. However, despite this general role, the effects of miR-145 can be context-dependent and even paradoxical, varying across different organs and pathological conditions. For example, while miR-145 exacerbates pulmonary fibrosis [30,31], it attenuates hepatic stellate cell-mediated fibrosis [32]. Even within the same organ, miR-145 may exert contrasting effects, such as impeding scar healing in the skin while promoting fibrosis in recessive dystrophic epidermolysis bullosa [33,34]. This functional versatility underscores the importance of cellular and pathological context in determining miR-145's effects. However, our research demonstrates that miR-145 is effective in improving erectile function in both senile ED [15,35]and senile nerve-injury ED, suggesting a consistent benefit across different etiologies of senile erectile dysfunction. Furthermore, recent work by Xiaolin Zhang et al. provides additional support for the pivotal role of miR-145 in ED treatment [36]. Their study revealed that mesenchymal stem cell-derived exosomes pretreated with melatonin mitigate cavernous fibrosis and improve erectile function in nerve injury-induced ED by delivering miR-145-5p. This independent validation further underscores the therapeutic significance of miR-145 in ED management and highlights its potential as a key molecular target for future interventions.

A central innovation of this study lies in the identification of the miR-145/TGFBR2 axis as the predominant mechanism underlying the therapeutic effects of Exo-145. Database mining, qPCR validation, and dual-luciferase assays identified TGFBR2 as a direct miR-145 target. As a pivotal TGF-β receptor, TGFBR2 drives fibrosis and apoptosis via the SMAD-dependent signaling pathway [37,38]. Earlier studies concluded that TGFBR2 knockdown inhibits liver fibrosis [39], while dominant-negative TβRII attenuates hypertrophic scarring [40]. Herein, miR-145 exerted anti-fibrotic effects by suppressing TGFBR2, thereby minimizing collagen deposition and CCSMC apoptosis post-injury.

Several limitations merit careful consideration. First, the absence of a dedicated lentiviral empty vector control group represents a design consideration. Including such a control is essential to distinguish non-specific effects resulting from lentiviral transduction, thus strengthening the evidence that the observed outcomes are specifically due to miR-145. Furthermore, while our findings highlight the therapeutic potential of Exo-145, it is important to recognize the physiological differences between rodent models and humans, which may limit the direct translatability of these results to clinical applications. Rigorous studies in larger preclinical models are crucial to thoroughly assess long-term safety, immunological effects, and potential off-target impacts. Addressing these gaps is critical for advancing Exo-145 from basic research to clinical application and ensuring its successful translation into therapeutic practice.

5. Conclusion

In summary, our multi-faceted approach reveals that Exo-145 effectively treats BCNI-induced ED in aged rats by delivering miR-145. This exosomal miRNA targets TGFBR2, leading to reduced cavernous apoptosis and fibrosis, and ultimately restoring erectile function (Fig. 7). These findings highlight the potential of exosome-mediated miR-145 delivery as a cell-free therapy for neurogenic ED, particularly in older populations, though further preclinical validation is essential.

Authors' contributions

Conceptualization: Hengjun Xiao, Hua Wang and Yunlong Ge. Data curation: Yude Hong, Zejia Feng and Yunlong Ge, Formal analysis: Yude Hong, Zejia Feng and Yunlong Ge. Funding acquisition: Hengjun Xiao. Investigation: Yude Hong, Zejia Feng and Yunlong Ge. Methodology: Yude Hong, Zejia Feng and Yunlong Ge. Supervision: Yuhang Xi and Jun Chen. Visualization: Jianjie Wu, Tian Xia, Bowen Tang and Wei Wang. Writing—original draft: Yude Hong, Zejia Feng, Yunlong Ge and Yuhang Xi. Writing—review & editing: Jun Chen, Hua Wang and Hengjun Xiao.

Declaration of Generative AI and AI-assisted technologies in the writing process

During the preparation of this work, the authors used generative AI tools (Gemini, ChatGPT, and DeepSeek) and native English-

speaking editors to refine the language and improve readability. After using these tools and services, the authors reviewed and edited the content as needed and take full responsibility for the content of the publication.

Funding

This study was supported by the National Natural Science Foundation of China (no. 81771573) and the Guangzhou Science and Technology Project (2024A03J0275).

Declaration of competing interest

The authors declare that they have no known competing financial interests or personal relationships that could have appeared to influence the work reported in this paper.

Acknowledgement

We thank the drawing tools provided by Figdraw. We would also like to express our gratitude to Dr. Weian Zhu for his thoughtful feedback and valuable suggestions during the review of the manuscript.

Appendix A. Supplementary data

Supplementary data to this article can be found online at https://doi.org/10.1016/j.reth.2025.04.004.

References

[1] Lue TF. Erectile dysfunction. N Engl J Med 2000;342:1802–13. https://doi.org/10.1056/NEJM200006153422407.
[2] Yafi FA, Jenkins L, Albersen M, Corona G, Isidori AM, Goldfarb S, et al. Erectile dysfunction. Nat Rev Dis Primers 2016;2:16003. https://doi.org/10.1038/nrdp.2016.3.
[3] Moretti TBC, Magna LA, Reis LO. Erectile dysfunction criteria of 131,350 patients after open, laparoscopic, and robotic radical prostatectomy. Andrology 2024;12:1865–71. https://doi.org/10.1111/andr.13634.
[4] EAU Guidelines. Sexual and reproductive health. ISBN 978-94-92671-23-3. In: Presented at the EAU annual congress. Paris: EAU Guidelines Office; 2024. Arnhem, The Netherlands. Available at: https://uroweb.org/guidelines.
[5] Samidurai A, Xi L, Das A, Kukreja RC. Beyond erectile dysfunction: CGMP-specific phosphodiesterase 5 inhibitors for other clinical disorders. Annu Rev Pharmacol Toxicol 2023;63:585–615. https://doi.org/10.1146/annurev-pharmtox-040122-034745.
[6] Daneshwar D, Lee Y, Nordin A. Stem cell assisted low-intensity shockwave for erectile dysfunction treatment: current perspective. Regen Ther 2024;26:1150–8. https://doi.org/10.1016/j.reth.2024.11.006.
[7] Al Hashimi M, Pinggera G-M, Mostafa T, Rambhatla A, Hamoda T, Shah R, et al. Regenerative therapy in erectile dysfunction: a survey on current global practice trends and GAF expert recommendations. World J Mens Health 2024. https://doi.org/10.5534/wjmh.240086.
[8] Hu D, Liu C, Ge Y, Ye L, Guo Q, Xi Y, et al. Poly-L-lactic acid/gelatin electrospun membrane-loaded bone marrow-derived mesenchymal stem cells attenuate erectile dysfunction caused by cavernous nerve injury. Int J Biol Macromol 2024;265:131099. https://doi.org/10.1016/j.ijbiomac.2024.131099.
[9] Ma L, Rao N, Jiang H, Dai Y, Yang S, Yang H, et al. Small extracellular vesicles from dental follicle stem cells provide biochemical cues for periodontal tissue regeneration. Stem Cell Res Ther 2022;13:92. https://doi.org/10.1186/s13287-022-02767-6.
[10] Wang B, Gao W, Zheng MY, Lin G, Lue TF. Recent advances in stem cell therapy for erectile dysfunction: a narrative review. Expet Opin Biol Ther 2023;23:565–73. https://doi.org/10.1080/14712598.2023.2203811.
[11] Welsh JA, Goberdhan DCI, O'Driscoll L, Buzas EI, Blenkiron C, Bussolati B, et al. Minimal information for studies of extracellular vesicles (MISEV2023): from basic to advanced approaches. J Extracell Vesicles 2024;13:e12404. https://doi.org/10.1002/jev2.12404.
[12] Lotfy A, AboQuella NM, Wang H. Mesenchymal stromal/stem cell (MSC)-derived exosomes in clinical trials. Stem Cell Res Ther 2023;14:66. https://doi.org/10.1186/s13287-023-03287-7.
[13] Long R, Wang S. Exosomes from preconditioned mesenchymal stem cells: tissue repair and regeneration. Regen Ther 2024;25:355–66. https://doi.org/10.1016/j.reth.2024.01.009.
[14] Liao H-J, Yang Y-P, Liu Y-H, Tseng H-C, Huo T-I, Chiou S-H, et al. Harnessing the potential of mesenchymal stem cells-derived exosomes in degenerative diseases. Regen Ther 2024;26:599–610. https://doi.org/10.1016/j.reth.2024.08.001.
[15] Liu Q, Cui Y, Lin H, Hu D, Qi T, Wang B, et al. MicroRNA-145 engineered bone marrowderived mesenchymal stem cells alleviated erectile dysfunction in aged rats. Stem Cell Res Ther 2019;10:398. https://doi.org/10.1186/s13287-019-1509-1.
[16] O'Brien J, Hayder H, Zayed Y, Peng C. Overview of MicroRNA biogenesis, mechanisms of actions, and circulation. Front Endocrinol 2018;9. https://doi.org/10.3389/fendo.2018.00402.
[17] Xi Y, Feng Z, Xia T, Hong Y, Wu J, Chen J, et al. Caveolin-1 scaffolding domain-derived peptide enhances erectile function by regulating oxidative stress, mitochondrial dysfunction, and apoptosis of corpus cavernosum smooth muscle cells in rats with cavernous nerve injury. Life Sci 2024;348:122694. https://doi.org/10.1016/j.lfs.2024.122694.
[18] Xi Y, Ge Y, Hu D, Xia T, Chen J, Zhang C, et al. Caveolin-1 scaffolding domain peptide prevents corpus cavernosum fibrosis and erectile dysfunction in bilateral cavernous nerve injury-induced rats. J Sex Med 2023:qdad108. https://doi.org/10.1093/jsxmed/qdad108.
[19] Ge Y, Hu D, Xi Y, Wang H, Xia T, Chen J, et al. An animal model induced by bilateral cavernous nerve crushing mimics post-radical prostatectomy erectile dysfunction in old rats. Life Sci 2023;325:121767. https://doi.org/10.1016/j.lfs.2023.121767.
[20] McGeary SE, Lin KS, Shi CY, Pham TM, Bisaria N, Kelley GM, et al. The biochemical basis of microRNA targeting efficacy. Science 2019;366:eaav1741. https://doi.org/10.1126/science.aav1741.
[21] Sticht C, De La Torre C, Parveen A, Gretz N. miRWalk: an online resource for prediction of microRNA binding sites. PLoS One 2018;13:e0206239. https://doi.org/10.1371/journal.pone.0206239.
[22] Chen Y, Wang X. miRDB: an online database for prediction of functional microRNA targets. Nucleic Acids Res 2020;48:D127–31. https://doi.org/10.1093/nar/gkz757.
[23] James N, Tannock I, N'Dow J, Feng F, Gillessen S, Ali SA, et al. The lancet commission on prostate cancer: planning for the surge in cases. Lancet 2024;403:1683–722. https://doi.org/10.1016/S0140-6736(24)00651-2.
[24] Siegel RL, Wagle NS, Cercek A, Smith RA, Jemal A. Colorectal cancer statistics, 2023. CA Cancer J Clin 2023;73:233–54. https://doi.org/10.3322/caac.21772.
[25] Sengupta P. The laboratory rat: relating its age with human's. Int J Prev Med 2013;4:624–30.
[26] Koga Y, Yasunaga M, Moriya Y, Akasu T, Fujita S, Yamamoto S, et al. Exosome can prevent RNase from degrading microRNA in feces. J Gastrointest Oncol 2011;2:215–22. https://doi.org/10.3978/j.issn.2078-6891.2011.015.
[27] Tan F, Li X, Wang Z, Li J, Shahzad K, Zheng J. Clinical applications of stem cell-derived exosomes. Signal Transduct Target Ther 2024;9:17. https://doi.org/10.1038/s41392-023-01704-0.
[28] Li J, Wang J, Chen Z. Emerging role of exosomes in cancer therapy: progress and challenges. Mol Cancer 2025;24:13. https://doi.org/10.1186/s12943-024-02215-4.
[29] Cordes KR, Sheehy NT, White MP, Berry EC, Morton SU, Muth AN, et al. miR-145 and miR-143 regulate smooth muscle cell fate and plasticity. Nature 2009;460:705–10. https://doi.org/10.1038/nature08195.
[30] Sun W, Zhou S, Peng L, Liu Y, Cheng D, Wang Y, et al. CircZNF609 regulates pulmonary fibrosis via miR-145-5p/KLF4 axis and its translation function. Cell Mol Biol Lett 2023;28:105. https://doi.org/10.1186/s11658-023-00518-w.
[31] Finotti A, Gasparello J, Fabbri E, Tamanini A, Corradini R, Dechecchi MC, et al. Enhancing the expression of CFTR using antisense molecules against MicroRNA miR-145-5p. Am J Respir Crit Care Med 2019;199:1443–4. https://doi.org/10.1164/rccm.201901-0019LE.
[32] Yang J, Lu Y, Yang P, Chen Q, Wang Y, Ding Q, et al. MicroRNA-145 induces the senescence of activated hepatic stellate cells through the activation of p53 pathway by ZEB2. J Cell Physiol 2019;234:7587–99. https://doi.org/10.1002/jcp.27521.
[33] Su J, Wei Q, Ma K, Wang Y, Hu W, Meng H, et al. P-MSC-derived extracellular vesicles facilitate diabetic wound healing via miR-145-5p/CDKN1A-mediated functional improvements of high glucose-induced senescent fibroblasts. Burns Trauma 2023;11:tkad010. https://doi.org/10.1093/burnst/tkad010.
[34] Condorelli AG, Logli E, Cianfarani F, Teson M, Diociaiuti A, El Hachem M, et al. MicroRNA-145-5p regulates fibrotic features of recessive dystrophic epidermolysis bullosa skin fibroblasts. Br J Dermatol 2019;181:1017–27. https://doi.org/10.1111/bjd.17840.
[35] Hu D, Ge Y, Xi Y, Chen J, Wang H, Zhang C, et al. MicroRNA-145 gene modification enhances the retention of bone marrow-derived mesenchymal stem cells within corpus cavernosum by targeting Krüppel-like factor 4. World J Mens Health 2024. https://doi.org/10.5534/wjmh.230149.
[36] Zhang X, Yang M, Chen X, Zhang M, Peng Y, Lu M. Melatonin-pretreated mesenchymal stem cell-derived exosomes alleviate cavernous fibrosis in a rat model of nerve injury-induced erectile dysfunction via miR-145-5p/TGF-β/smad axis. Stem Cell Res Ther 2025;16:96. https://doi.org/10.1186/s13287-025-04173-0.
[37] Deng Z, Fan T, Xiao C, Tian H, Zheng Y, Li C, et al. TGF-β signaling in health, disease, and therapeutics. Signal Transduct Target Ther 2024;9:61. https://doi.org/10.1038/s41392-024-01764-w.
[38] Gu JJ, Li HX, Wei W, Sun XL, Li BC, Chen Y, et al. Bone marrow mesenchymal stem cell transplantation alleviates radiation-induced myocardial fibrosis through inhibition of the TGF-β1/Smad2/3 signaling pathway in rabbit model. Regen Ther 2023;24:1–10. https://doi.org/10.1016/j.reth.2023.04.003.

[39] Wang Y, Du J, Niu X, Fu N, Wang R, Zhang Y, et al. MiR-130a-3p attenuates activation and induces apoptosis of hepatic stellate cells in nonalcoholic fibrosing steatohepatitis by directly targeting TGFBR1 and TGFBR2. Cell Death Dis 2017;8:e2792. https://doi.org/10.1038/cddis.2017.10.

[40] Reid RR, Roy N, Mogford JE, Zimmerman H, Lee C, Mustoe TA. Reduction of hypertrophic scar via retroviral delivery of a dominant negative TGF-beta receptor II. J Plast Reconstr Aesthetic Surg 2007;60:64–72. https://doi.org/10.1016/j.bjps.2005.12.026. discussion 73-74.